Smart Structures and Systems, *Vol. 24, No. 4 (2019) 475-490*
DOI: https://doi.org/10.12989/sss.2019.24.4.475

Baseline-free damage detection method for beam structures based on an actual influence line

Ning-Bo Wang[1a], Wei-Xin Ren[2b] and Tian-Li Huang[*1]

[1]*School of Civil Engineering, Central South University, Changsha 410075, China*
[2]*Department of Civil Engineering, Hefei University of Technology, Hefei 230009, China*

(Received March 19, 2019, Revised June 9, 2019, Accepted June 10, 2019)

Abstract. The detection of structural damage without a priori information on the healthy state is challenging. In order to address the issue, the study presents a baseline-free approach to detect damage in beam structures based on an actual influence line. In particular, a multi-segment function-fitting calculation is developed to extract the actual deflection influence line (DIL) of a damaged beam from bridge responses due to a passing vehicle. An intact basis function based on the measurement position is introduced. The damage index is defined as the difference between the actual DIL and a constructed function related to the intact basis, and the damage location is indicated based on the local peak value of the damage index curve. The damage basis function is formulated by using the detected damage location. Based on the intact and damage basis functions, damage severity is quantified by fitting the actual DIL using the least-square calculation. Both numerical and experimental examples are provided to investigate the feasibility of the proposed method. The results indicate that the present baseline-free approach is effective in detecting the damage of beam structures.

Keywords: baseline-free; damage detection; beam structure; multi-segment function; actual influence line

1. Introduction

It is very important to detect damage prior to the occurrence of a catastrophic event. This allows for the assessment of structural safety during the service period and determination of time intervals for conducting maintenance. Damage detection based on modal parameters and related derived indices is widely examined (Alvandi and Cremona 2006, Ren and Roeck 2012a, b, Yan *et al*. 2007), including the power mode shape (Fang and Perera 2009), modal strain energy (Yang *et al*. 2012), mode shape curvature (Wang *et al*. 2014, Cao and Xu 2014, 2015), and flexibility curvature (Tomaszewska 2010, Jaishi and Ren 2006). Recently, Zhang *et al*. (2012) proposed a damage location detection method based on the mode shape square (MOSS) by introducing a sinusoidal tapping force on a moving vehicle. The aforementioned modal based damage detection methods are effective when the accuracy of dynamic parameters is guaranteed, which typically requires a lot of sensors and is considered time-consuming and costly. Nevertheless, it is difficult to obtain accurate modal parameters and especially high-order mode information. Furthermore, modal based techniques require either a baseline or a mathematical model of the undamaged structure that is unrealistic for existing structures.

*Corresponding author, Professor
E-mail: htianli@csu.edu.cn
[a] Associate Professor
E-mail: wangnb@csu.edu.cn
[b] Professor
E-mail: renwx@hfut.edu.cn

The use of signal processing (e.g., time-frequency analysis)-based damage detection is also widespread in recent decades. Zhu and Law (2006) used a wavelet transform for the crack identification of beam structures from a deflection response, which localizes the crack from the sudden change in the spatial variation of the transform responses. Roveri and Carcaterra (2012) adopted the Hilbert-Huang transform (HHT) of a displacement response for damage localization based on the peak of instantaneous frequency. Hester and Gonzalez (2012) developed a wavelet-based damage detection algorithm based on bridge acceleration responses. Li and Hao (2015) applied a continuous wavelet transform and HHT to analyze the relative displacement response and successfully identified the damage of shear connectors in a composite bridge. A promising advantage of the aforementioned signal processing based approaches is that they do not rely on simulation models. The damage is visualized through the appearance of singularity in a processed signal that is considered as smooth in the intact state. However, the quantification of damage persists as an issue given the lack of definite correspondence between the adopted damage index and damage severity.

An increasing amount of research interest is focused on damage detection implementations based on the interactive system of moving vehicle and beam structures. Vehicle induced responses are close to the actual condition and always exhibit a high signal-to-noise ratio (SNR). Gonzalez and Hester (2013) numerically investigated the damage to a beam based on bridge acceleration responses due to a vehicle by introducing a moving average filter (MAF) to remove the 'dynamic' component and retain the 'damage' curve. However, the effect of road unevenness and multi-axle vehicle was not included. Zhang *et al*. (2017) developed a phase trajectory that was established by displacement, velocity, and acceleration

ISSN: 1738-1584 (Print), 1738-1991 (Online)

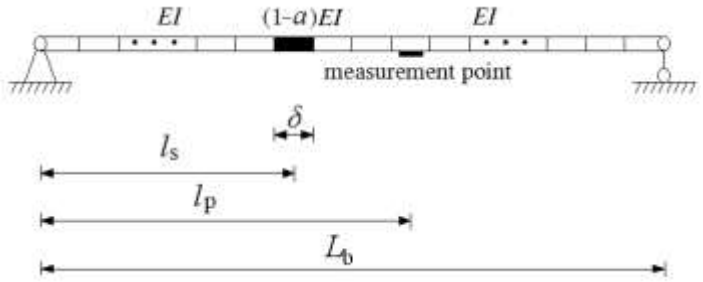

Fig. 1 Simply supported beam model with local damage

responses of a measurement point and defined the damage index as the phase trajectory change before and after damage. Its damage index is significantly influenced by bridge surface conditions, and the damage position could be confused by vehicle axles. Similarly, He *et al*. (2017a) conducted damage localization and quantification of beam structures from the change in displacement. Chen *et al.* (2015) proposed a damage localization method of a suspension bridge by using the stress response change. These two methods consider the dynamic response as an influence line by applying a quasi-static moving load or considering the vehicle as the point load, and a uniform vehicle velocity is assumed.

However, the aforementioned damage detection algorithms require baseline information. Modal based and response based methods always require the exact mode shape or response curve under healthy state. And the signal processing based approaches assume a smooth characteristic as the generalized baseline.

A new idea that is gradually developed in damage detection involves constructing baseline information from the damaged state. A gapped smoothing method (GSM) and a global fitting method (GFM) by Yoon *et al*.(2005, 2009) were applied to the mode shape from damaged structures to obtain a spline shape interpolation that describes a healthy state. Subsequently, Zhang *et al*. (2013) used the GFM for the damage detection of beam structure based on the operating deflection shape curvature (ODSC) that considers the modified ODSC as the substitution of the intact state. The method includes a complex sinusoidal tapping force acting on the passing vehicle. He *et al*. (2017b) proposed a baseline-free damage localization method for statically determinate beam structures by using dual-type responses (strain and displacement) under a quasi-static moving load. The baseline information of displacement response is estimated through the strain response in the current state by assuming that it remains constant when subjected to local damages. In addition to the requirement for an extremely high accurate strain measurement, the method has a few limitations such as the measurement point must be set at the undamaged region and the distance between the measurement point and the neutral axis of the beam must be given. Furthermore, only damage localization is referred to in the method. Based on the aforementioned statement, it is challenging to obtain exact intact information (mode shape and response) from the current state.

In the present study, a damage detection method without baseline information is developed for statically determinate beam structures. A multi-segment function is used to model and extract the actual DIL of the damaged beam structure. An intact basis function based on the measurement position is introduced. Subsequently, the damage index is defined as the difference between the actual DIL and the constructed function related to the intact basis, and the damage location is indicated based on the local peak value in the damage index curve. The damage basis functions are formulated by using the detected damage location. Additionally, based on the two types of basis functions, the damage severity is quantified by fitting the actual DIL. Numerical examples of a vehicle crossing a simply-supported beam are included to investigate the accuracy of DIL extraction, damage localization, and quantification. Furthermore, the effect factor of damage identification is investigated. The validity and feasibility of the proposed method is further verified by conducting an experimental study.

2. DIL extraction of damaged beam structure

A two-segment piece-wise polynomial function is proven as effective in fitting the actual IL in a previous study (Wang *et al*. 2017a). The method is only suitable for beam structures with a constant flexural rigidity, and thus it is unsuitable for beams containing a non-uniform flexural rigidity. The present study involves a further extension of DIL extraction for a damaged beam structure.

Fig. 1 presents a simply supported beam with length L_b with flexural rigidity *EI* of the undamaged section and (1 - α) *EI* of the damaged section. Variable α is a flexural rigidity reduction factor where $0 \le \alpha < 1$. The measurement point position l_P, damage location l_S, and damage region (l_s - δ/2, l_s + δ/2) are also shown. Based on the principle of virtual displacement, the DIL of a measurement point corresponds to the deflection curve caused by a unit force acting at the corresponding position, and its theoretical expression can be derived. When the unit force acts at the measurement section l_P, the bending moment of beam structure is as follows

$$M_P(X)=\begin{cases}-\frac{l_P}{L_b}X+X & 0\le X\le l_P\\ -\frac{l_P}{L_b}X+l_P & l_P<X\le L_b\end{cases} \quad (1)$$

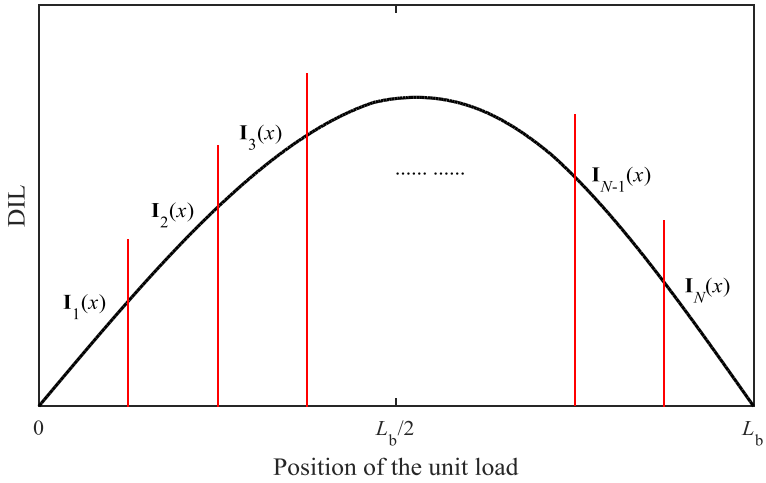

Fig. 2 Multi-segment DIL model

Assuming that a unit force acting at position x, the bending moment influence line (BMIL) of a random section X is

$$\overline{M}(x,X)=\begin{cases}-\dfrac{x}{L_b}X+X & (0\le X\le x)\\ -\dfrac{x}{L_b}X+x & (x\le X\le L_b)\end{cases} \tag{2}$$

Taking the beam structure shown in Fig. 1 as an example, the deflection curve which can also considered as the DIL of measurement point is derived as follows

$$\mathrm{DIL}(x)=\int_0^{L_b}\frac{M_p(X)\overline{M}(x,X)}{EI(X)}dX=\mathrm{DIL}_0(x)+\Delta\mathrm{DIL}(x) \tag{3a}$$

$$\mathrm{DIL}_0(x)=\frac{1}{EI}\int_0^{L_b}M_p(X)\overline{M}(x,X)dX=\begin{cases}f_1(x) & x\le l_p\\ f_2(x) & x>l_p\end{cases} \tag{3b}$$

$$\Delta\mathrm{DIL}(x)=\left(\frac{1}{(1-\alpha)}-1\right)\frac{1}{EI}\int_{l_s-\delta/2}^{l_s+\delta/2}M_p(X)\overline{M}(x,X)dX=\begin{cases}g_1(x) & x\le l_s-\delta/2\\ g_2(x) & l_s-\delta/2<x\le l_s+\delta/2\\ g_3(x) & x>l_s+\delta/2\end{cases} \tag{3c}$$

The detailed definition of Eqs. (3(b)) and (3(c)) is specified in Appendix A.

According to Eq. (3), the DIL of damaged beam structure actually corresponds to the piece-wise cubic polynomial function with several segments that separate at the location of the measurement point and damage position.

Actually, for beams with a general boundary condition (i.e., existing rotation stiffness at each end), the DIL can also be represented by using the piece-wise cubic polynomial function (Wang *et al*. 2017a). It should be noted that a two-segment piece-wise polynomial that segments at the known measurement point is only suitable to describe the DIL of the undamaged beams. Additionally, the present study further extends the previous fitting method of IL extraction to the damaged beam structures by introducing a multi-segment function that can reserve the damage information and accurately describes the DIL.

A piece-wise function model $\mathbf{I}$ is utilized to describe the DIL of the damaged state that includes a series of cubic polynomials. As shown in Fig. 2, the DIL is approximately divided into N segments along the bridge length, the i^{th} segment of DIL is described by $\mathbf{I}_i$ (i=1, 2, ..., N), and function $\mathbf{I}$ is given as follows

$$\mathbf{I}=[\mathbf{I}_1,\ \mathbf{I}_2,\ \ldots,\ \mathbf{I}_{N-1},\ \mathbf{I}_N] \tag{4}$$

where $\mathbf{I}_i=a_ix^3+b_ix^2+c_ix+d_i$, the variables a_i, b_i, c_i, and d_i denote the coefficients of $\mathbf{I}_i$, and x in $\mathbf{I}_i$ relates to the starting and ending points of the i^{th} segment.

Herein, a segment exhibits uniform flexural rigidity, but different segments can exhibit different flexural rigidities to simulate unknown damage. The segment number N is extended to the maximum possible extent to ensure that the damage region is contained in a segment or several adjacent segments. Furthermore, the two adjacent segments must be continuous and first order and second order derivable. Additionally, the starting value of the first segment $\mathbf{I}_1$ is zero as it is the ending value of the last segment $\mathbf{I}_N$. The continuous conditions and boundary conditions are expressed as follows

$$\begin{cases}\mathbf{I}_i\left(x=\dfrac{L_b}{N}i\right)=\mathbf{I}_{i+1}\left(x=\dfrac{L_b}{N}i\right)\\ \mathbf{I}_i'\left(x=\dfrac{L_b}{N}i\right)=\mathbf{I}_{i+1}'\left(x=\dfrac{L_b}{N}i\right)\\ \mathbf{I}_i''\left(x=\dfrac{L_b}{N}i\right)=\mathbf{I}_{i+1}''\left(x=\dfrac{L_b}{N}i\right)\\ \mathbf{I}_1(0)=0;\qquad \mathbf{I}_N(L_b)=0\end{cases}\quad i=(1,2,\cdots,N-1) \tag{5}$$

By using derivations described in Wang *et al*. (2017a), the vector $\mathbf{I}$ in Eq. (4) is utilized to fit the quasi-static part of the bridge response due to the moving load, and a series of harmonic sinusoids are established to describe the fluctuation part that exists in the response.

It is assumed that the bridge dynamic response of measurement point is a result of the passage of a multi-axle vehicle with known information, i.e., axle weights m_i, wheelbase D_i, and vehicle speed v. The data sequence

during the first axle arriving at the bridge and last axle leaving bridge is selected and denoted as ***R***. The quasi-static part and the fluctuation part are individually fitted by $\widetilde{R}_S$ and $\widetilde{R}_D$, respectively, and expressed as follows

$$\widetilde{R}_S = \sum_{i=1}^{num} m_i \mathbf{P}(x - \mathrm{D}_i)\mathbf{I}(x - \mathrm{D}_i) \tag{6}$$

$$\widetilde{R}_D = \sum_n \left(\frac{-S_n}{(1-S_n^2)} \sum_{i=1}^{num} m_i \left(\sin(w_n(t-t_{p_i}))\mathbf{H}(t-t_{p_i}) + \sin(w_n(t-t_{q_i}))\mathbf{H}(t-t_{q_i}) \right) \right) \cdot \boldsymbol{\psi}_n \tag{7}$$

where P(·) denotes the rectangular window function, and H(·) denotes the Heaviside step function. Both are used to describe the behavior of arriving and leaving bridge for the vehicle axles. And the other variables were described in the previous study (Wang *et al.* 2017a).

$$\mathrm{P}(z) = \begin{cases} 1 & 0 \le z \le L_b \\ 0 & else \end{cases} \tag{8}$$

$$\mathrm{H}(z) = \begin{cases} 1 & z \ge 0 \\ 0 & z < 0 \end{cases} \tag{9}$$

Subsequently, the response data sequence ***R*** is collectively fitted by $\widetilde{R}_S$ and $\widetilde{R}_D$, the coefficients a_i, b_i, c_i, d_i in the vector **I** and coefficient $\boldsymbol{\psi}_n$ of the fluctuation part are obtained through the least-square calculation. Additionally, the DIL of a damaged beam structure comprised of multi-segments is obtained.

It is concluded that the multi-segment function fitting method is also suitable for undamaged structures and beams with uneven flexural rigidity. Its feasibility is verified through numerical and experimental studies in the subsequent sections.

3. IL based damage detection methodology

3.1 Intact information construction

In damage localization, the damage index is defined as the difference between the current information of the damaged state and exact information of the undamaged state, such as the difference in the phase trajectories formed by three types of responses (displacement, velocity, and acceleration) (Zhang *et al*. 2017), stress influence line (SIL) (Chen *et al*. 2015), displacement responses (He *et al*. 2017a, b), and mode shape and its related parameters (Wang *et al*. 2014, Cao and Xu 2014, 2015, Zhang *et al*. 2013). The baseline information included in the aforementioned methods is mainly obtained from the healthy state. Additionally, a few smoothing methods are used to obtain the baseline from the data of the current state.

The exact baseline information, which is always difficult to accurately obtain, is not included in the damage detection approach. Herein, a function containing the intact features is developed instead and termed as 'intact basis function'.

Generally, the bending moment of a statically determinate beam structure is irrelevant to local damages. When the unit force acts at the measurement point, the bending moment M_p is given in Eq. (1). Additionally, an intact basis function ξ_0 representing the intact information is constructed as follows

$$\xi_0(x) = \int_0^{L_b} M_p(X)\overline{M}(x,X)dX \tag{10}$$

where $\overline{M}(x,X)$ denotes the bending moment of the beam under a unit virtual force applied at position x ($0 \le x \le L_b$), and it changes with respect to the variable x.

Evidently, the basis function is easily constructed for a given measurement point since it is unrelated to the flexural rigidity of intact state. ξ_0 is not equal to the exact deflection influence line of the undamaged state ($\mathrm{DIL}^{\mathrm{u}}$). However, it is not difficult to determine that ξ_0 exhibits the same shape as $\mathrm{DIL}^{\mathrm{u}}$, and a proportionality exists between them.

3.2 Damage localization

Given the aforementioned multi-segment function fitting calculation, the actual influence line of the damaged structure ($\mathrm{DIL}^{\mathrm{d}}$) is extracted from the bridge responses under moving loads. In conjunction with the constructed intact basis function ξ_0, the damage index DI is defined as follows

$$\mathrm{DI} = \mathrm{DIL}^{\mathrm{d}} - \lambda \cdot \xi_0 \tag{11}$$

where $\mathrm{DIL}^{\mathrm{d}}$ and ξ_0 denote the damage information and intact information, respectively. The exact intact DIL information $\mathrm{DIL}^{\mathrm{u}} = \xi_0/EI$, while EI is always unknown during the damage detection. Another coefficient λ is introduced and corresponds to the ratio of the area encircled by $\mathrm{DIL}^{\mathrm{d}}$ and the horizontal axis to that encircled by ξ_0 and the horizontal axis, and it is expressed as follows

$$\lambda = \frac{\int_0^{L_b} DIL^{\mathrm{d}}(x)dx}{\int_0^{L_b} \xi_0(x)dx} \tag{12}$$

Evidently, the area encircled by the damage index curve and the horizontal axis is zero. When the beam structure does not exhibit damage, $\lambda = 1/EI$, and $DI = \mathbf{0}$. Additionally, if the local damage exists as shown in Fig. 3, the value of damage index gradually increases while approaching the damage region and forms a local peak. Thus, the position of local peak point of the damage index indicates the damage location.

3.3 Damage severity identification

With respect to the beam structure shown in Fig. 1, the DIL of any measurement point slightly increases after damaged. In theory, the change in DIL before and after damage is expressed as follows

$$\Delta DIL(x) = DIL^{\mathrm{d}}(x) - DIL^{\mathrm{u}}(x) = \left(\frac{1}{1-\alpha} - 1 \right) \frac{1}{EI} \int_{l_S-\delta/2}^{l_S+\delta/2} M_p(X)\overline{M}(x,X)dX \tag{13}$$

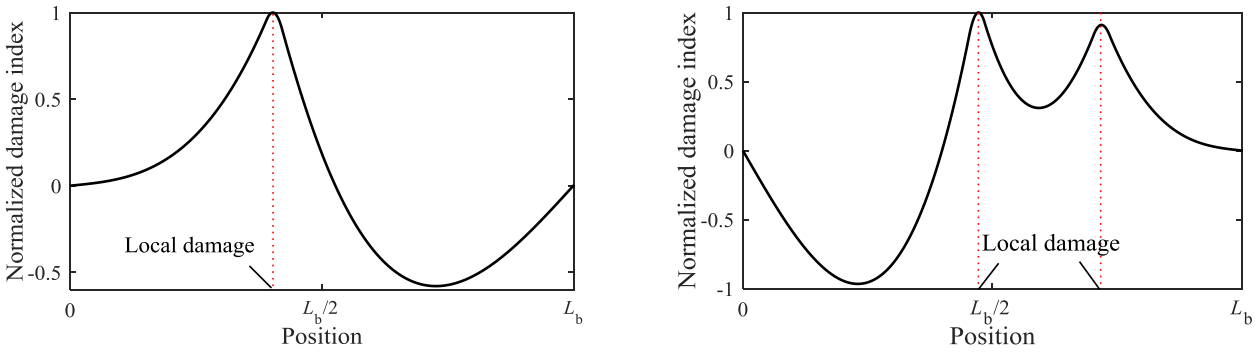

(a) Single damage (b) Double damage

Fig. 3 Theoretical damage index curves of different damage scenarios

With respect to Eq. (1), the bending moment $\overline{M}$ is sectional linear as is the M_p. Additionally, the damage region δ typically exhibits a small size. Thus, it satisfies the following expression

$$\int_{l_S-\delta/2}^{l_S+\delta/2} M_p(X)\overline{M}(x,X)dX \approx \delta\, M_p(l_S)\overline{M}(x,l_S) \tag{14}$$

where

$$\overline{M}(x,l_S)=\begin{cases}-\dfrac{1}{L_b}l_S x+l_S & 0\le l_S\le x\\ -\dfrac{1}{L_b}l_S x+x & x<l_S\le L_b\end{cases} \tag{15}$$

Subsequently, Eq. (13) is approximated as follows

$$\Delta\mathrm{DIL}\approx\delta\left(\frac{1}{1-\alpha}-1\right)\frac{1}{EI}M_p(l_S)\begin{cases}-\dfrac{1}{L_b}l_S x+x & 0\le x\le l_S\\ -\dfrac{1}{L_b}l_S x+l_S & l_S<x\le L_b\end{cases} \tag{16}$$

Assuming that

$$\xi_1=M_p(l_S)\begin{cases}-\dfrac{1}{L_b}l_S x+x & 0\le x\le l_S\\ -\dfrac{1}{L_b}l_S x+l_S & l_S<x\le L_b\end{cases} \tag{17}$$

$$\beta_0=\frac{1}{EI} \tag{18}$$

$$\beta_1=\delta\left(\frac{1}{1-\alpha}-1\right)\frac{1}{EI} \tag{19}$$

With respect to the beam structure with single damage, the $\mathrm{DIL}^{\mathrm{d}}$ is expressed as follows

$$\mathrm{DIL}^{\mathrm{d}}=\beta_0\xi_0+\beta_1\xi_1 \tag{20}$$

For the multi-damage situation, the following expression is applicable

$$\xi_i=M_p(l_{Si})\begin{cases}-\dfrac{1}{L_b}l_{Si}x+x & 0\le x\le l_{Si}\\ -\dfrac{1}{L_b}l_{Si}x+l_{Si} & l_{Si}<x\le L_b\end{cases} \tag{21}$$

$$\beta_i=\delta_i\left(\frac{1}{1-\alpha_i}-1\right)\frac{1}{EI}\qquad i=(1,2,\cdots,n) \tag{22}$$

Then, the $\mathrm{DIL}^{\mathrm{d}}$ is expressed as follows

$$\mathrm{DIL}^{\mathrm{d}}=\beta_0\xi_0+\beta_1\xi_1+\cdots+\beta_n\xi_n \tag{23}$$

where n denotes the number of damages, and δ_i and α_i denote the length of damage region and flexural rigidity reduction factor of the i^{th} local damage, respectively.

$\mathrm{DIL}^{\mathrm{d}}$ denotes the actual influence line of beam structure that can be obtained by the proposed method in Section 2. Specifically, ξ_0 is considered as an intact basis function and ξ_i (i=1, 2, ..., n) denotes the damage basis functions. The results evidently indicate that ξ_0 is a constant vector that is related to the measurement position l_{P}, and ξ_i is related to the measurement position l_{P} and the damage location l_S. The actual coefficients β_0, β_1, ..., and β_{n} are obtained by solving Eq. (23) through the least-square method. Subsequently, the flexural rigidity reduction factor α_i and flexural rigidity EI of the intact state are determined by a combined solution of Eqs. (18) and (22) and are expressed as follows:

$$\frac{\alpha_i}{1-\alpha_i}\delta_i=\frac{\beta_i}{\beta_0}\qquad i=(1,2,\cdots,n) \tag{24}$$

$$EI=\frac{1}{\beta_0} \tag{25}$$

It should be noted that the damage severity in the study describes the flexural rigidity reduction within a region. Only when the damage region δ_i is given, the reduction factor α_i is established from Eq. (24). The aforementioned property is adopted in several studies (Zhang *et al.* 2012, 2013, Zhang *et al.* 2017, He *et al.* 2017a, b) and uses the stiffness reduction of the given length elements for a quantitative description of the damage.

4. Numerical studies

This section uses the numerical examples of vehicle–bridge interaction to validate the DIL extraction method in Section 2 and the damage detection method in Section 3. A

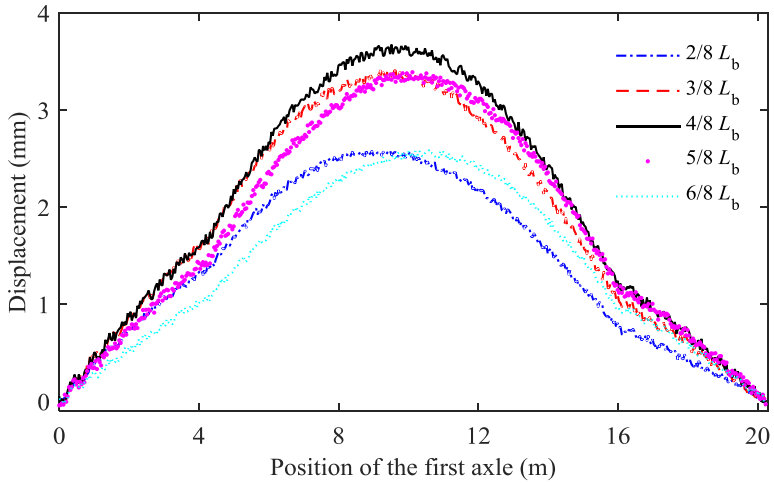

Fig. 4 Calculated dynamic responses in the single damage scenario

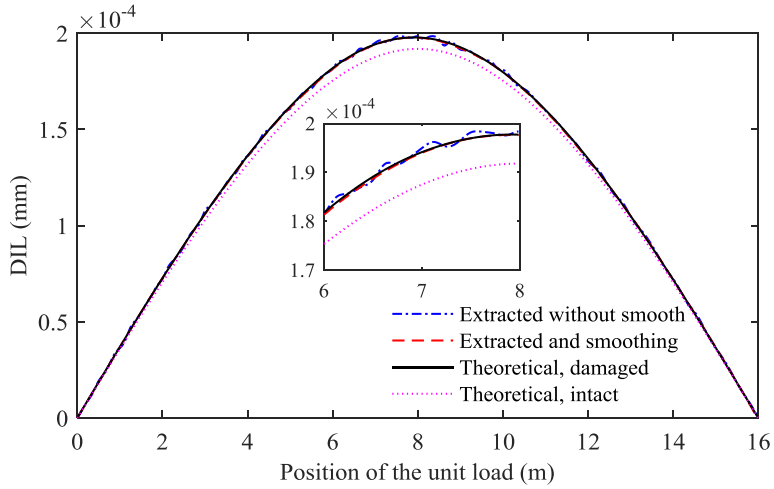

Fig. 5 Comparison of extracted DIL and the theoretical curves of the point at the mid-span

simply supported beam structure is adopted. The properties of the beam are: length L_b = 16 m, linear density 1.07×10^4 kg/m, and flexural rigidity $EI = 4.36\times10^9$ N·m^2. Rayleigh damping is considered with a damping ratio of 0.02. A 2-axle vehicle model is adopted, and the detailed parameters are given in Zhu and Law (2003). The interaction process is simulated by finite element method with numerical software (MATLAB). Two damage scenarios are considered in the numerical simulation: (1) single-damage in the location l_S = 6.5 m with δ = 1 m and α = 0.2; and (2) double-damage in locations l_{S1} = 7.5 m and l_{S2} = 11.5 m with δ_1 = 1 m, α_1 = 0.3, and δ_2 = 1 m and α_2 = 0.2, respectively.

The time step of implicit integration in vehicle-bridge interaction simulation is 0.001 s, and the output frequency of simulated response is 100 Hz. The relatively low vehicle speed with the average of 2 m/s is adopted to ensure the accuracy of DIL extraction. Thus, the road surface irregularity is ignored in the low speed situation. The white noise is introduced and added to the displacement response when extracting the DIL.

4.1 DIL extraction of damaged beam

Theoretically, damage localization and damage quantification is implemented based on only a single measurement point by the proposed approach. Specifically, the displacement responses of five points at $2/8L_b$, $3/8L_b$, $4/8L_b$, $5/8L_b$, and $6/8L_b$ are individually used for damage detection.

Fig. 4 shows the typical dynamic responses of the five sections induced by the passing of the 2-axle vehicle model that are under a vehicle velocity of 2 m/s and contaminated by 5% noise. Based on the dynamic responses, the actual DIL of the five measurement points are extracted by the fitting calculation discussed in Section 2.

The segment number n = 64 is selected in the piece-wise function **I** to describe the DIL of the damaged state. A MAF (Sayers and Karamihas 1996) process is used to smooth out short-term fluctuation disturbance that exists in DIL by the fitting calculation. Specifically, the discrete points included in the range of a segment (0.25 m) are averaged.

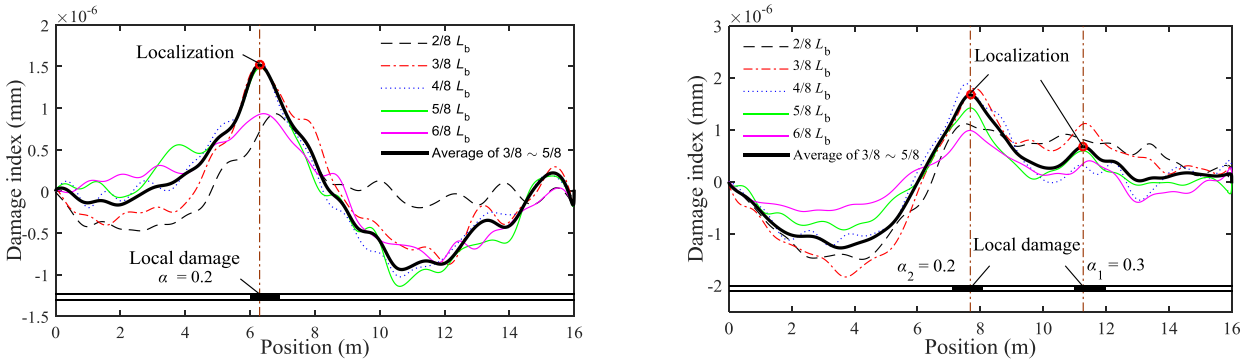

(a) Single damage scenario (b) Double damage scenario

Fig. 6 Damage index for measurement points at different locations

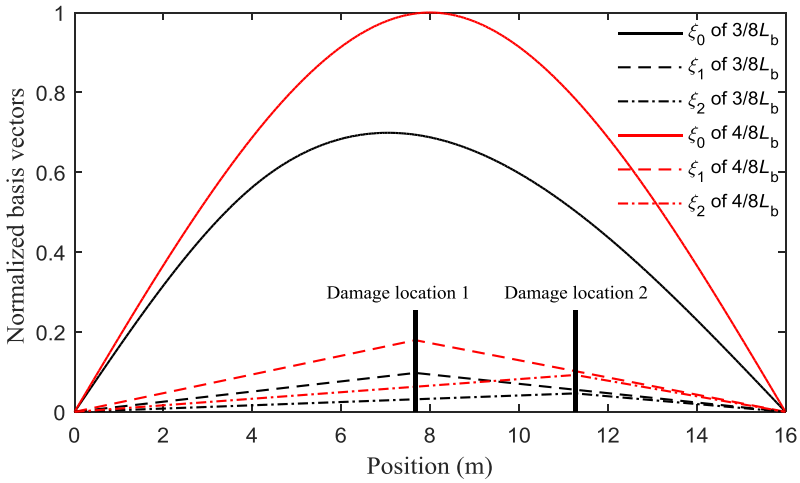

Fig. 7 Basis functions of the measurement points at $3/8L_b$ and $4/8L_b$

Considering the measurement point $4/8L_b$ as an example, the extracted DIL, smoothed curve, and theoretical curves of the damaged and intact state are compared in Fig. 5. As shown in the figure, the extracted DIL effectively retains the damage information, and it includes slight disturbances, but the smoothed DIL by a simple MAF almost coincides with the theoretical curve.

Thus, the proposed DIL extraction method of damaged beam structure is feasible. The MAF process is necessary to eliminate the slight disturbance and improves the accuracy of the DIL based damage detection.

4.2 Damage detection

As mentioned in Section 3, the damage localization and quantification is implemented based on the extracted DIL of the damaged state, i.e., DIL^d. The intact basis function ξ_0 of each measurement point is constructed based on its position. The damage index is subsequently established by combining the DIL^d and ξ_0.

Figs. 6 (a) and 6(b) show the damage index curves of two damage scenarios at different locations. It should be noted that for these two damage scenarios, the damage index of the point close to the mid-span (e.g., $3/8L_b$-$5/8L_b$) exhibits an evident amplitude while the point of the two sides (e.g., $2/8L_b$, $6/8L_b$) produces a relatively flat damage index curve. Specifically, the three points at $3/8L_b$, $4/8L_b$, and $5/8L_b$ are used for damage localization by determining the peak value point from the averaged curve. The detected damage locations are shown in Fig. 6, and all of these are extremely close to the real damage positions.

Based on the detected damage location, the damage basis function ξ_i (i=1, 2, ...) is obtained. With respect to the single damage scenario, by substituting DIL^u, ξ_0 and ξ_1 into Eq. (16) to solve for coefficients β_0 and β_1 based on the least-square principle, the flexural rigidity reduction factor α is subsequently identified. With respect to the double damage scenario, only an additional basis function ξ_2 is included, and Eq. (19) is used for the coefficient solution.

Considering the double damage scenario as an example, the basis functions ξ_0, ξ_1, and ξ_2 of measurement points at different locations are plotted in Fig. 7. As shown in Fig. 7, the value of the three basis functions of the same position are always at the same level, ξ_0 relies on the location of the measurement point, and ξ_1 and ξ_2 are collectively determined by the measurement point position and corresponding damage location. The calculated components relying on each basis are shown in Fig. 8(a). Evidently, the

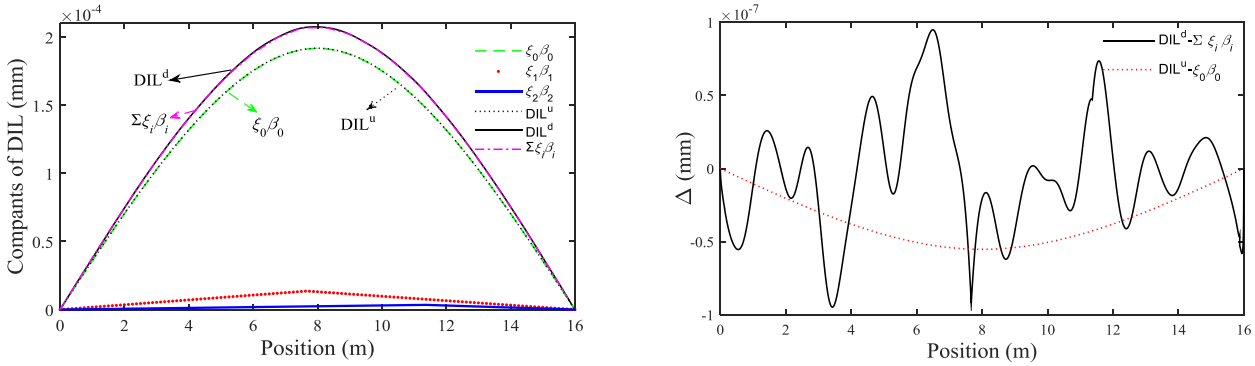

(a) Double damage scenario (b) Difference

Fig. 8 Comparison of identified components and DILs of the point at $4/8L_b$

Table 1 Damage detection results in the numerical studies

M. P. location	Scenario 1: single damage			Scenario 2: double damage				
	l_S (m)	α	EI_0/EI	l_{S1} (m)	l_{S2} (m)	α_1	α_2	EI_0/EI
2/8 L_b	/	0.189	0.998	/	/	0.301	0.186	1.002
3/8 L_b		0.187	0.998			0.293	0.202	1.002
4/8 L_b	6.37	0.182	0.996	7.63	11.34	0.295	0.195	0.999
5/8 L_b		0.172	0.995			0.282	0.193	1.000
6/8 L_b	/	0.170	0.996	/	/	0.296	0.188	1.002
Averaged	6.37	0.180	0.997	7.63	11.34	0.293	0.193	1.001
True	6.5	0.2	1	7.5	11.5	0.3	0.2	1

Note: EI_0 denotes the identified flexural rigidity of beam in the intact state, and l_S, l_{S1}, and l_{S2} are established by the average value of the damage index of three points at $3/8L_b \sim 5/8L_b$.

intact component $\beta_0\xi_0$ coincides with the DIL^u of the healthy state, the damage components $\beta_1\xi_1$ and $\beta_2\xi_2$ are evident, and the sum of $\beta_i\xi_i$ (i = 0, 1, 2) coincides with the damaged influence line DIL^d. In order to obtain a clear expression, the difference between these two curves is plotted in Fig. 8(b) that presents an extremely small deviation.

The damage detection results are listed in Table 1. As shown in the table, the detected damage location and damage severity of two scenarios are close to the assumed values, and the flexural rigidity of beam structure in the intact state can also be accurately identified. The measurement points at $3/8L_b$-$5/8L_b$ are adequately used for damage detection individually and especially for damage quantification.

4.3 Effects discussion

4.3.1 Segment number in DIL extraction

The influence line based damage detection method proposed in the study contains three steps in order, namely DIL extraction, damage localization, and damage severity identification. Thus, the extraction of the actual DIL information from the bridge responses due to a passing vehicle plays an important role. In addition to the requirement of the high-quality response signal, the number of segments is a critical parameter in the DIL extraction. Factually, the piece-wise cubic function is considered as a specific filter that is used to eliminate interference and obtain a quasi-static tendency. A multi-segment function can describe the DIL of the damaged state accurately and reserve damage information. The more the segments are divided, the better the damage information is described although its filtering effect is weaker. Thus, a reasonable segment number is required. In the numerical study, the number of segments N satisfies that L_b/N = 0.25 m. With respect to the case of the small damage region, a large segment number is adopted.

Despite the simple MAF method is confirmed as capable of eliminating the slight perturbation that exists in the calculated DIL. It should be noted that a large segment number results in a large matrix equation in the inverse calculation of the coefficients of DIL. Additionally, the regularization method is recommended for solving the ill-posed problem (Chen 2008) and is prone to achieve a satisfactory result even from the response with evident noise and vibration interference.

4.3.2 Testing condition

Generally, vehicle velocity and testing noise are the major factors involved in the proposed damage detection method. A relatively low vehicle speed was recommended

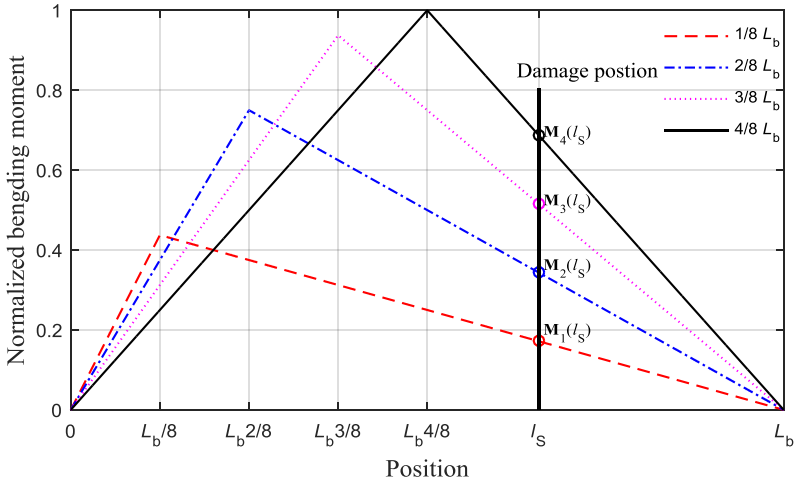

Fig. 9 Bending moment diagrams by the unit force acting at four sections

in the signal based damage identification by several studies (Zhang *et al.* 2012, 2013). In the present study, a low velocity condition is also desirable to significantly reduce the interference of road unevenness. Non-uniform velocity is another effect factor, but it was perfectly described in the influence line extraction in a previous study (Wang *et al.* 2017a).

The noise effect may be contained in the extracted DIL while using a multi-segment function, since the piece-wise cubic function with large number of segments plays a minor role in signal filtering. Generally, numerous segments are required to ensure the adequacy of damage information while the effect of noise is inevitable. Based on the aforementioned numerical example, the MAF process eliminates the non-smoothness of DIL curve when 5% Gaussian white noise is considered in the responses. A further calculation performed by the authors indicates that a noise level exceeding 10% significantly affects the implementation of the damage detection and especially results in an evident deviation in the damage location. Additionally, the low-pass filtering method is proven as prone to the loss of damage information although it can completely filter the noise.

Thus, the testing noise of bridge dynamic responses should be maintained at a low level by using a sophisticated instrument. Additionally, for the same condition, a heavy vehicle is recommended to obtain responses with high SNR.

4.3.3 Location of measurement points

The DIL exhibiting a significant change between the damaged and intact states is beneficial for damage detection, and this implies that the measurement points with a higher damage basis function are more suitable under the same damage situation. It is concluded from Eqs. (1) and (17) that the damage basis function of each measurement point is related to the value $M(l_S)$ that represents the bending moment of the damage section under a unit load. The normalized bending moment diagrams induced by unit force acting at points $1/8L_b$-$4/8L_b$ are plotted in Fig. 9.

As shown in Fig. 9, the unit force acting at points $3/8L_b$ and $4/8L_b$ generates an evidently higher $M(l_S)$ value for most damage locations. Additionally, while acting at $1/8\ L_b$, it always exhibits the smallest $M(l_S)$ value unless the damage position is close to it. Based on symmetry, the measurement points at $3/8L_b$-$5/8L_b$ are preferred for the damage detection method, and points at $2/8L_b$ and $6/8L_b$ are also acceptable.

4.3.4 Damage features

As discussed in Section 3, the difference between DIL^d and DIL^u is determined by the damage features (i.e., damage location and damage severity). The single damage that occurs near the mid-span produces a higher DIL deviation and is thus prone to be detected. With respect to the single damage situation, several types of damage severity are defined by the flexural rigidity reduction factor to analyze the damage effect. The above 2-axle vehicle model and damaged simply supported beam are re-used for analyzing damage effects, and the measurement points at $3/8L_b$, $4/8L_b$, and $5/8L_b$ are adopted for damage localization by considering an average. Normalized damage index curves with seven different damage severity values are plotted in Fig. 10 wherein the result of the previous scenario 1 is assumed as a reference for normalization. As shown in the figure, it is easier to capture higher damage severity through the proposed damage index in the study. The damage with a flexural rigidity reduction factor $\alpha \geq 0.10$ is well identified. Slight damage with $\alpha \leq 0.05$ results in a flat damage index curve, and the peak point corresponding to the damage location is always obscured.

Furthermore, with respect to the multiple damage situations, the shape of damage index curve depends on the reduction factors of each damage point. Figs. 11(a) and 11(b) present the theoretical damage index curves of a double damage situation and triple damage situation, respectively. The results suggest that the damages with the same severity are indicated equally. With respect to multiple damage cases with different severity values, the point with a higher flexural rigidity reduction factor corresponds to a high

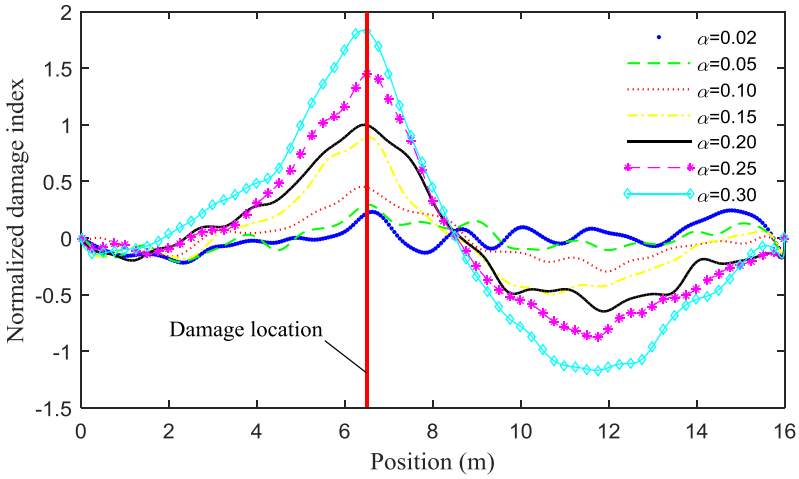

Fig. 10 Comparison of the damage index curves for different damage severity values

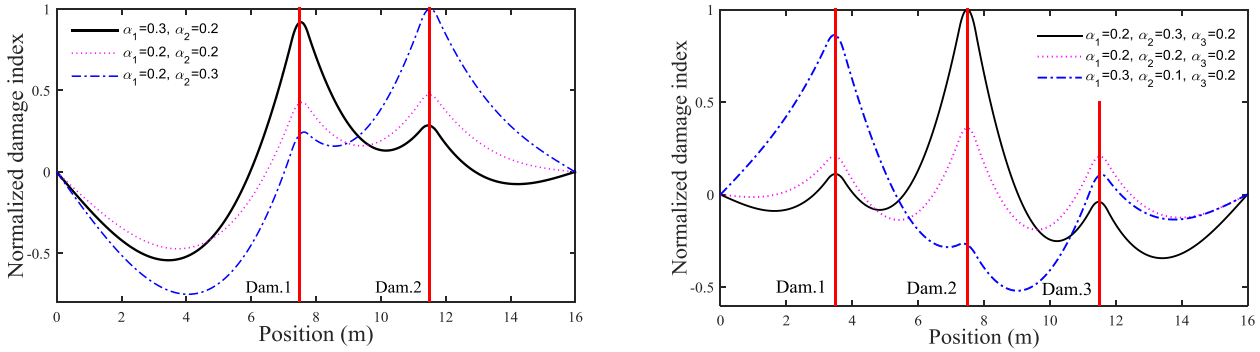

(a) Two damages (b) Three damages

Fig. 11 Three-points-averaged damage index curves of multiple damage cases

damage index value, and a slight-damage point corresponds to a low damage index value that can be possibly submerged.

5. Experimental verification

In order to further verify the validity and feasibility of the proposed damage detection method, a simply supported beam with leading and tailing beams is utilized in the experimental study.

5.1 Experimental setup

An experimental setup that simulates the behavior of a vehicle arriving and leaving a bridge is shown in Fig. 12. A laser range finder is utilized to test the real-time velocity of the model vehicle by manually dragging through a traction rope. The bridge model (testing beam) includes a 5.0 m long simply supported steel beam with a 100 mm × 68 mm × 4.5 mm I-shape section. A similar auxiliary beam is utilized for supporting the model vehicle and is parallel to the testing beam, and the transverse distance between two beams is 0.258 m. A single damage case (DP_2) with damage region δ = 0.15 m, flexural rigidity reduction factor α = 0.42-0.45, and a double damage case (DP_1, DP_2) with damage region δ_1 = 0.15 m, δ_2 = 0.15 m, flexural rigidity reduction factor α_1 = 0.28-0.30, and α_2 = 0.42-0.45 are arranged in the test beam. The actual flexural rigidity reduction factors are estimated from several sections in each artificial damage region that are gained by cutting part of the lower flange of the I-beam. Two measurement points (MP_1 and MP_2) are set near the mid-span. The exact positions of damage regions, measurement points, and the damage sizes are denoted in Fig. 13(a). The measured fundamental frequency of the test beam in healthy state is 14.75 Hz. A box-type vehicle model as shown in Fig. 13(b) is utilized, and its total mass is adjusted by changing the load on the vehicle. Three 'V' shape wheels are fixed on the carriage model to simulate a constant axle weight during running, and the weight of each wheel is measured in a static condition. In the study, the axle weights of m_1=16.7 kg, m_2=8.55 kg, and m_3=8.56 kg that result in a bridge response with high SNR are selected. The model vehicle acts on two independent beams, namely a test beam with artificial damage and an auxiliary beam that supports a smooth guide rail for the 'V' shape wheel. Specifically, a 2-axle vehicle and a single-axle vehicle are individually

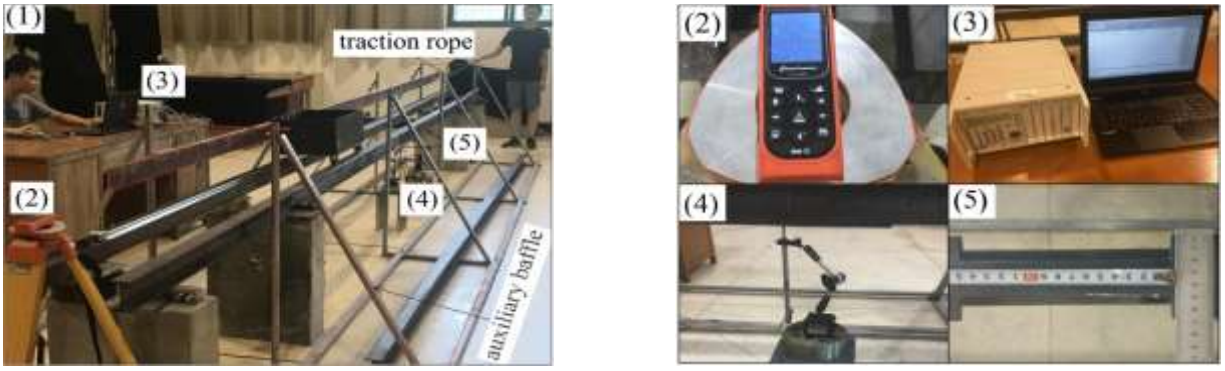

Fig. 12 Components of the experiment model: (1) global view of the test; (2) laser range finder; (3) HBM data collection system; (4) displacement sensor: WA20; (5) local damage (150 mm×20 mm×2 mm)

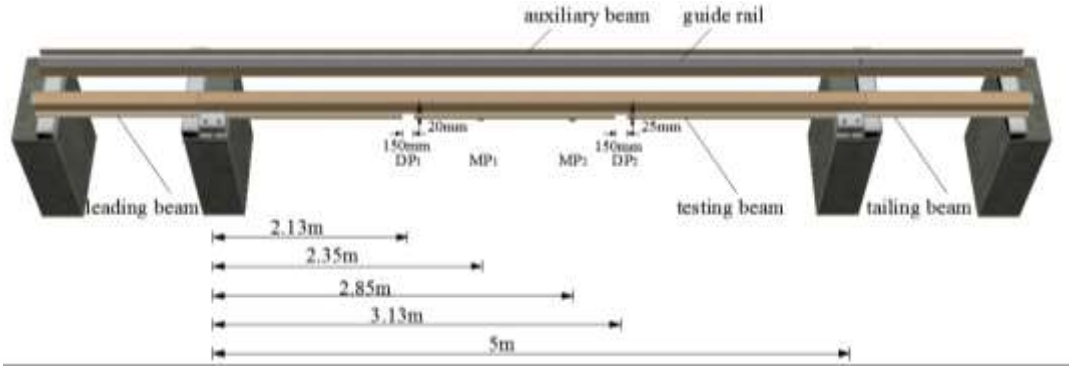

(a) Bridge model and arrangements

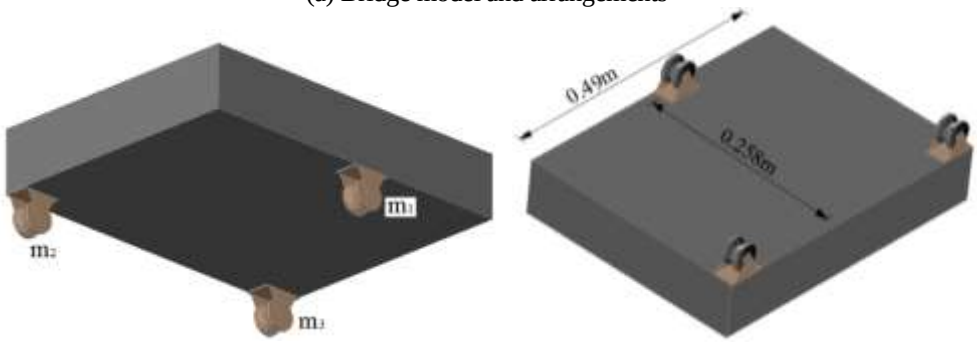

(b) Vehicle model

Fig. 13 Experimental setup of the simply supported beams under the moving vehicle

simulated by the model. An auxiliary baffle is also installed outside the two beams to ensure the straight movement of the model vehicle on the beams.

Both static loading and dynamic loading are involved in the experiment. The static load cases are used to directly obtain accurate IL information, in which the point load is realized by the single-wheel side of the vehicle model. Additionally, the dynamic load by the double-wheel side, i.e., a 2-axle vehicle model, is used to produce continuous response data for DIL extraction and damage detection. An HBM data collection system (MGCPlus) is used in the test, and two displacement sensors are included. A sampling frequency of 5 Hz is adopted for static loading, and a sampling frequency of 100 Hz is adopted for dynamic loading.

5.2 DIL in damaged state

The static test by single point load is first conducted to obtain the value of a discrete IL curve that is considered as the real IL of the damaged beam. The positions of each static loading point are approximately uniform along the bridge, and the exact values are from the laser range finder. Similarly, the instantaneous positions of vehicle model are recorded in the dynamic test. Fig. 14(a) plots the length travel and velocity curves wherein the data for travel length and time point are from continuous records by the laser range finder, and the real-time velocity is acquired through the difference calculation. Fig. 14(b) presents the corresponding displacement responses due to the passage of the vehicle model. Subsequently, the responses between

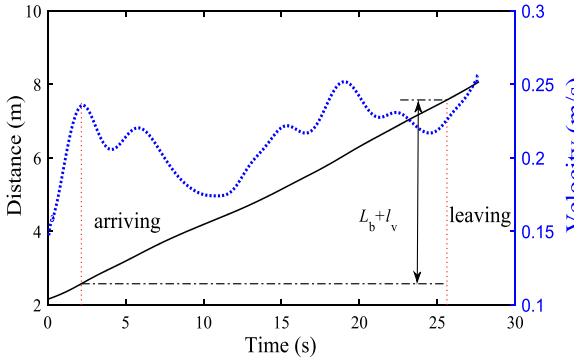

(a) Length travel and velocity curves

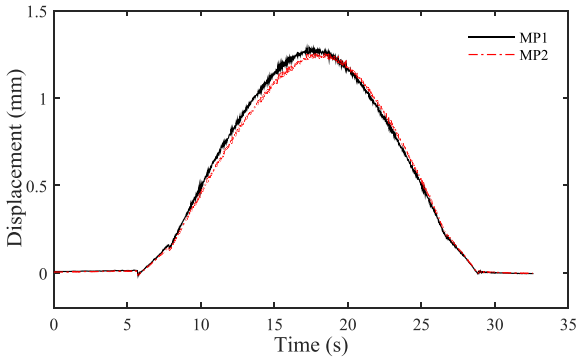

(b) Measured data under a moving 2-axle vehicle model

Fig. 14 Measured data under a moving 2-axle vehicle model

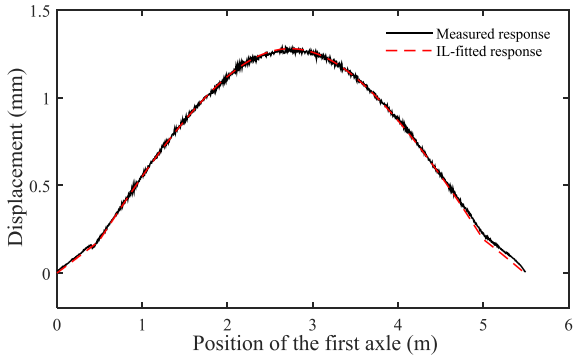

(a) Response fitting

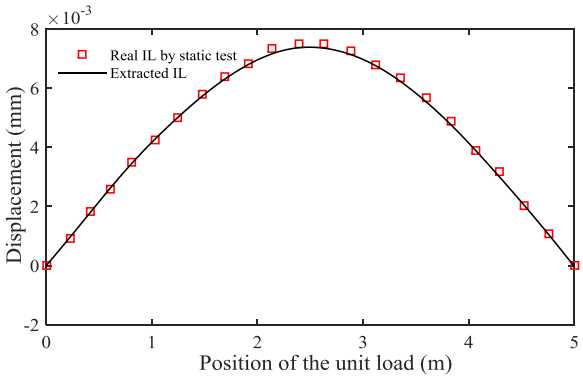

(b) ILs

Fig. 15 Comparison of the responses and ILs of MP_1

arriving and leaving points are selected for IL extracting.

The multi-segment function with segment number N = 50 is used in fitting the response. The fitted curve and measured response of MP_1 are compared in Fig. 15(a). As shown in the figure, the multi-segment function can effectively fit the response while introducing a real-time velocity. Considering the single damage case as an example, the extracted DIL curve and discrete point of the real IL from the static loading are compared in Fig. 15(b). A simple MAF is applied to the extracted DIL, and a high coincidence exists between the extracted DIL curve and real IL discrete points by the static test. Thus, the effectiveness of the DIL extraction algorithm in the study is verified.

5.3 Damage detection results

The damage index is obtained based on the above extracted DIL curves and the intact basis function related to the position of the measurement point, and the damage location is subsequently indicated by its peak point. The damage index curves of two cases and the identified damage locations are shown in Figs. 16(a) and 16(b), respectively. Specifically, the local peak point that indicates the damage location is evident in the damage index curve. The damage index curve of the double damage case may include a few non-evident peak points that just reflect a slight slope change and do not clearly indicate the peak position. A wavelet-based approach is proposed to establish the aforementioned peak points (Wang et al. 2017b; Chatterjee *et al*. 2006). The damage basis function based on the damage position is setup and used for the quantification analysis. Fig. 17 shows all the components referred in damage quantification, which include the fitted DIL curve and actual DIL curve of the damaged state, intact DIL obtained in the fitting calculation, and the damage effects. As shown in the figure, the fitted DIL coincides with the actual DIL curve extracted from the testing responses. The actual damage effect that corresponds to the calculated difference between the actual DIL and intact DIL matches well with the superposition of the fitted damage parts. Specifically, all the damage effects are enlarged five times for a clear observation.

Table 2 shows a comparison of the damage location, damage severity, and the flexural rigidity of the I-shape beam. The actual length of damage region may exceed the assumed value of 0.15 m in the identifying calculation, and this implies that the damage quantification is arranged in a relatively small region. Thus, the identified damage severity may exceed the actual estimated value. Nevertheless, the identified result essentially coincides with the actual value, which verifies the validity and feasibility of the damage detection method. The exact intact information of DIL is

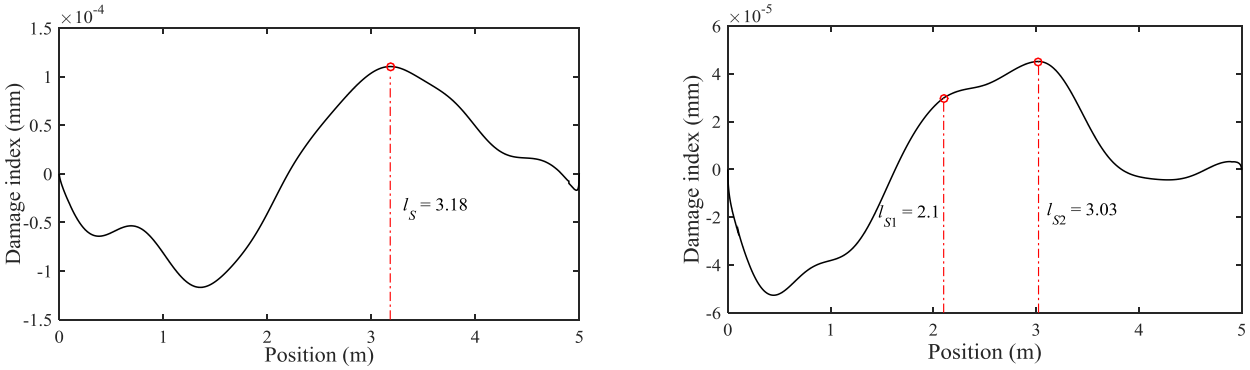

(a) Single damage case (b) Double damage case

Fig. 16 Averaged damage index curves of different cases from the two measurement points

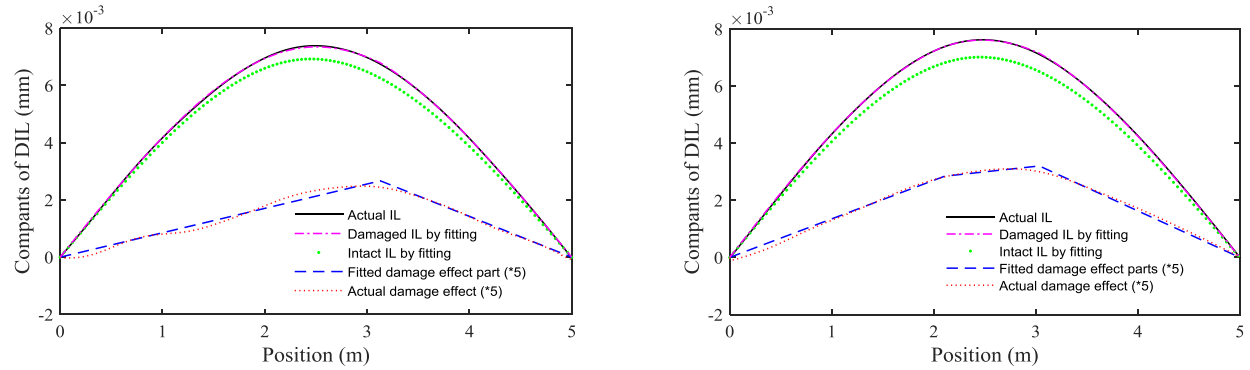

(a) Single damage case (b) Double damage case

Fig. 17 Components referred in the damage quantification of different cases of MP_1

Table 2 Damage detection results of the model experiment

	Single damage case			**Double damage case**				
	Damage position	Damage severity	Flexural rigidity	Damage position		Damage severity		Flexural rigidity
	l_S (m)	α	EI_0/EI	l_{S1} (m)	l_{S2} (m)	α_1	α_2	EI_0/EI
Identified	3.18	0.53	0.995	2.10	3.03	0.30	0.48	0.989
Actual value	3.13	0.42~0.45	1	2.13	3.13	0.28~0.30	0.42~0.45	1

Note: EI_0 denotes the identified flexural rigidity of the I shape beam in the intact state. The actual flexural rigidity EI of tested beam is based on fundamental frequency testing in the intact state and an inverse calculation from $f = 1/2\pi\sqrt{EI/mL^4}$, where f = 14.75 Hz denotes the tested fundamental frequency, L = 5.0 m denotes the bridge length, and m = 6.8235 kg/m represents the linear density that is obtained by the weight measurement.

obtained during the fitting calculation while the flexural rigidity EI_0 in the intact state is also identified. The values of EI_0 gained from two damage cases are nearly identical and approximately equal to the real value EI obtained from a frequency measurement in the intact state. All the aforementioned facts also indirectly illustrate the accuracy of the damage detection method.

6. Conclusions

The study proposes a baseline-free damage detection method for statically determinate beam structures based on an actual influence line. The DIL extracted from bridge responses by a multi-segment function fitting calculation is a static feature curve that contains damage information. When compared to the response curve, the DIL is not affected by the non-uniform vehicle speed, testing noise,

road unevenness, and multi axles and is considered as an ideal index for damage detection. Basis functions representing the intact information and damage information are individually introduced for damage localization and damage severity identification. The basis function describing intact information is not the exact baseline curve (DIL^u) that is always difficult to accurately obtain from the damaged state. However, it exhibits the same shape and is in proportion to the baseline. The intact basis function ξ_0 is obtained easily and is superior to the generalized baseline that is considered as smooth in signal processing based damage detection approaches.

The damage location is indicated by the damage index established based on the actual DIL and intact basis function. Subsequently, the damage basis function is defined, and damage severity is identified through a fitting calculation by using the basis functions. Only a single measurement point is required for damage detection in the proposed method. It is proven that $3/8L_b$-$5/8L_b$ denotes the ideal position for the measurement point irrespective of where the damage occurs. Furthermore, the actual DIL is a major factor related to damage detection, and the bridge response with high SNR is desired to guarantee accurate DIL extraction.

The feasibility of the proposed damage detection approach and DIL extraction method by a multi-segment function is verified through numerical and experiment studies. It should be noted that the proposed baseline free method is only suitable for statically determinate beams. Future work is dedicated to damage detection bridges with non-uniform cross-sections and/or more complicated boundary conditions.

Acknowledgments

The study is supported by National Science Foundation of China with Grant nos. 51508576 and 51478472. This support is gratefully acknowledged. The authors also express their sincere gratitude to the reviewers for their valuable comments and suggestions.

References

Alvandi, A. and Cremona, C. (2006), "Assessment of vibration-based damage identification techniques", *J. Sound Vib.*, **292**(1-2), 179-202. https://doi.org/10.1016/j.jsv.2005.07.036.

Chatterjee, P., O'Brien, E.J., Li Y. and González, A. (2006), "Wavelet domain analysis for identification of vehicle axles from bridge measurements", *Comput. Struct.*, **84**(28), 1792-1801. https://doi.org/10.1016/j.compstruc.2006.04.013.

Chen, H.P. (2008), "Application of regularization methods to damage detection in large scale plane frame structures using incomplete noisy modal data", *Eng. Struct.*, **30**(11), 3219-3227. ttps://doi.org/10.1016/j.engstruct.2008.04.038.

Cao, M., Radzieński, M., Xu, W. and Ostachowicz, W. (2014), "Identification of multiple damage in beams based on robust curvature mode shapes", *Mech. Syst. Signal Pr.*, **46**(2), 468-480. https://doi.org/10.1016/j.ymssp.2014.01.004.

Chen, Z.W., Zhu, S.Y., Xu, Y.L., *et al.* (2015), "Damage detection in long suspension bridge using stress influence lines", *J. Bridge Eng.*, **20**(3), 05014013 1-13. https://doi.org/10.1061/(ASCE)BE.1943-5592.0000681.

Fang, S.E. and Perera, R. (2009), "Power mode shapes for early damage detection in linear structures", *J. Sound Vib.*, **324**(1-2), 40-56. https://doi.org/10.1016/j.jsv.2009.02.002.

Gonzalez, A. and Hester, D. (2013), "An investigation into the acceleration response of a damaged beam-type structure to a moving force", *J. Sound Vib.*, **332**(13), 3201-3217. https://doi.org/10.1016/j.jsv.2013.01.024.

Hester, D. and Gonzalez, A. (2012), "A wavelet-based damage detection algorithm based on bridge acceleration response to a vehicle", *Mech. Syst. Signal Pr.*, **28**(2), 145-166. https://doi.org/10.1016/j.ymssp.2011.06.007.

He, W.Y., Ren, W.X. and Zhu, S. (2017a), "Damage detection of beam structures using quasi-static moving load induced displacement response", *Eng. Struct.*, **145**(15), 70-82. https://doi.org/10.1016/j.engstruct.2017.05.009.

He, W.Y., Ren, W.X. and Zhu, S. (2017b), "Baseline-free damage localization method for statically determinate beam structures using dual-type response induced by quasi-static moving load", *J. Sound Vib.*, **400**(21), 58-70. https://doi.org/10.1016/j.jsv.2017.03.049.

Jaishi, B. and Ren, W.X. (2006), "Damage detection by finite element model updating using modal flexibility residual", *J. Sound Vib.*, **290**(1-2), 369-387. https://doi.org/10.1016/j.jsv.2005.04.006.

Li, J. and Hao, H. (2015), "Damage detection of shear connectors under moving loads with relative displacement measurements", *Mech. Syst. Signal Pr.*, **60-61**, 124-150. https://doi.org/10.1016/j.ymssp.2014.09.014.

Ren W. X., Roeck G. D. (2002a), "Structural damage identification using modal data. I: simulation verification", *J. Struct. Eng.*, **128**(1), 87-95. https://doi.org/10.1061/(ASCE)0733-9445(2002)128:1(87).

Ren, W.X. and Roeck, G.D. (2002b), "Structural damage identification using modal data. II: test verification", *J. Struct. Eng.*, **128**(1), 96-104. https://doi.org/10.1061/(ASCE)0733-9445(2002)128:1(96).

Roveri, N. and Carcaterra, A. (2012), "Damage detection in structures under traveling loads by Hilbert-Huang transform", *Mech. Syst. Signal Pr.*, **28**(2), 128-144. https://doi.org/10.1016/j.ymssp.2011.06.018.

Sayers, M.W. and Karamihas, S.M. (1996), "Interpretation of road roughness profile data-final report", *University of Michigan Transportation Research Institute (UMTRI) Report*, 96-19.

Tomaszewska, A. (2010), "Influence of statistical errors on damage detection based on structural flexibility and mode shape curvature", *Comput. Struct.*, **88**(3-4), 154-164. https://doi.org/10.1016/j.compstruc.2009.08.017.

Wang, Y., Liang, M. and Xiang, J. (2014), "Damage detection method for wind turbine blades based on dynamics analysis and mode shape difference curvature information", *Mech. Syst. Signal Pr.*, **48**(1-2), 351-367. https://doi.org/10.1016/j.ymssp.2014.03.006.

Wang, N.B., He, L.X., Ren, W.X. and Huang, T.L. (2017a), "Extraction of influence line through a fitting method from bridge dynamic response induced by a passing vehicle", *Eng. Struct.*, **151**: 648-664. https://doi.org/10.1016/j.engstruct.2017.06.067.

Wang, N.B., Ren, W.X. and Chen, Z.W. (2017b), "Wavelet-based automatic identification method of axle distribution information", *Struct. Eng.Mech.*, **63**(6), 761-769. https://doi.org/10.12989/sem.2017.63.6.761.

Xu, W., Cao, M., Ostachowicz, W., *et al.* (2015), "Two-dimensional curvature mode shape method based on wavelets and Teager energy for damage detection in plates", *J. Sound*

Vib., **347**, 266-278. https://doi.org/10.1016/j.jsv.2015.02.038.
Yoon, M.K., Heider, D., Jr J.W.G., *et al*. (2005), "Local damage detection using the two-dimensional gapped smoothing method", *J. Sound Vib.*, **279**(1-2), 119-139. https://doi.org/10.1016/j.jsv.2003.10.058.
Yan, Y.J., Cheng, L., Wu, Z.Y., *et al.* (2007), "Development in vibration-based structural damage detection technique", *Mech. Syst. Signal Pr.*, **21**(5), 2198-2211. https://doi.org/10.1016/j.ymssp.2006.10.002.
Yoon, M.K., Heider, D., Jr J.W.G., *et al*. (2009), "Local damage detection with the global fitting method using mode shape data in notched beams", *J. Nondestruct. Eval.*, **28**(2), 63-74.
Yan, W.J., Ren, W.X. and Huang, T.L. (2012), "Statistic structural damage detection based on the closed-form of element modal strain energy sensitivity", *Mech. Syst. Signal Pr.*, **28**(2), 183-194. https://doi.org/10.1016/j.ymssp.2011.04.011.
Zhu, X.Q. and Law, S.S. (2003), "Identification of moving interaction forces with incomplete velocity information", *Mech. Syst. Signal Pr.*, **17** (6), 1349-1366. https://doi.org/10.1006/mssp.2002.1577.
Zhu, X.Q. and Law, S.S. (2006), "Wavelet-based crack identification of bridge beam from operational deflection time history", *Int. J. Solids Struct.*, **43**(7-8), 2299-2317. https://doi.org/10.1016/j.ijsolstr.2005.07.024.
Zhang, Y., Wang, L. and Xiang, Z. (2012), "Damage detection by mode shape squares extracted from a passing vehicle", *J. Sound Vib.*, **331**(2), 291-307. https://doi.org/10.1016/j.jsv.2011.09.004.
Zhang, Y., Seng, T.L. and Xiang, Z. (2013), "Damage detection method based on operating deflection shape curvature extracted from dynamic response of a passing vehicle", *Mech. Syst. Signal Pr.*, **35**(1-2), 238-254. https://doi.org/10.1016/j.ymssp.2012.10.002.
Zhang, W., Li, J., Hao, H., *et al.* (2017), "Damage detection in bridge structures under moving loads with phase trajectory change of multi-type vibration measurements", *Mech. Syst. Signal Pr.*, **87**, 410-425. https://doi.org/10.1016/j.ymssp.2016.10.035.

HJ

Appendix A

$$f_1(x)=\frac{(L_b-l_p)}{6L_bEI}x^3+\frac{(l_p^3+3L_bl_p^2-2L_b^2l_p)}{6L_bEI}x \tag{A.1}$$

$$f_2(x)=-\frac{l_p}{6L_bEI}x^3+\frac{l_p}{2EI}x^2-\frac{(l_p^3+2L_b^2l_p)}{6L_bEI}x+\frac{l_p^3}{6EI} \tag{A.2}$$

$$g_1(x)=\frac{\left(\delta^3+12\delta l_s^2-12\delta L_b l_s\right)\left(L_b-l_p\right)}{12\alpha EIL_b^2}x \tag{A.3}$$

$$g_2(x)=\frac{\left(L_b-l_p\right)}{6\alpha EIL_b}x^3+\frac{\left(2\delta^3-3L_b\delta^2+24\delta l_s^2-12L_b\delta l_s-12L_bl_s^2\right)\left(L_b-l_p\right)}{24\alpha EIL_b^2}x-\frac{\left(L_b\delta^3-6L_bl_s\delta^2+12L_b\delta l_s^2-8L_bl_s^3\right)\left(L_b-l_p\right)}{24\alpha EIL_b^2} \tag{A.4}$$

$$g_3(x)=\frac{\left(\delta^3+12\delta l_s^2\right)\left(L_b-l_p\right)}{12\alpha EIL_b^2}x-\frac{\left(\delta^3+12\delta l_s^2\right)\left(L_b-l_p\right)}{12\alpha EIL_b} \tag{A.5}$$